Macromolecules

pubs.acs.org/Macromolecules Article

Compositionally Controlled Polyether Membranes via Mono(μ-alkoxo)bis(alkylaluminum)-Initiated Chain-Growth Network Epoxide Polymerization: Synthesis and Transport Properties

Christina G. Rodriguez, Malgorzata Chwatko, Jaesung Park, Caitlin L. Bentley, Benny D. Freeman,* and Nathaniel A. Lynd*

Cite This: *Macromolecules* 2020, 53, 1191−1198 Read Online

ACCESS | Metrics & More | Article Recommendations | Supporting Information

ABSTRACT: The addition of a diglycidyl-ether to a mono(μ-alkoxo)bis(alkylaluminum)-initiated epoxide polymerization presents a strategy for amorphous polyether-based membrane synthesis. In situ kinetic ^{1}H NMR spectroscopy was used to monitor model network copolymerizations of epichlorohydrin (ECH) with 1,4-butanediol-diglycidyl ether (Butyl-dGE) or poly(ethylene oxide)-diglycidyl ether (PEO-dGE). Reactivity ratios were extracted from the evolution of polymer composition from the monomer feed during copolymerization. Quantitative conversion and nearly random comonomer incorporation was achieved. The generality of this synthetic technique was supported by the polymerization of Butyl-dGE and a range of epoxide monomers such as *n*-butyl glycidyl ether (*n*BGE), allyl glycidyl ether, ECH, and glycidol. The copolymerizations produced optically clear, flexible films in all cases. We investigated the potential for this synthetic platform to provide compositional control of structure−property relationships within the context of industrially relevant membrane separations for CO_2. Given the affinity of PEO for CO_2 and water, we explored using *n*BGE as a hydrophobic diluent, which was copolymerized with varying incorporations of PEO-dGE. The resultant cross-linked polyether membranes exhibited high CO_2 permeabilities (150−300 barrer) and selectivity over N_2 (α_{CO_2/N_2} = 20−30) and H_2 ($\alpha_{CO_2/H_2} \approx 6$). CO_2 sorption isotherms could be described by Henry's law and did not vary across the series of *n*BGE/PEO-dGE films. The similar sorption coefficients suggested that differences in permeability among these samples were driven by differences in diffusion coefficients. The diffusivity of CO_2 increased with cross-link density, and permeability was unaffected by humidity for this series of hydrophobic cross-linked polyether membranes.

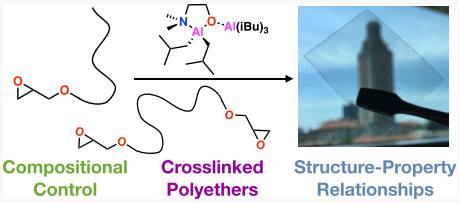

INTRODUCTION

Polyethers, derived from epoxides, are capable of providing compositional control of structure−property relationships when more than one monomer is combined into a single polymer backbone.[1−3] This compositional versatility addresses technological needs in biomedical applications, polymer electrolytes, antifouling and fouling release coatings, and membrane separations.[4−8] Polyethers are of particular interest because of the polar ether oxygen linkages present in their backbone, which exhibit favorable interactions with ions, CO_2, and other small molecules such as pharmaceutical agents.[9−11] The abundance of commercially available epoxide monomers provides a wide range of functionality that can be further modified to achieve desirable physical and chemical properties for targeted applications.

Poly(ethylene oxide) (PEO) is an especially attractive membrane material for light gas separations involving CO_2 or other acid or polar/quadrupolar gases, but PEO can crystallize, which reduces permeability and mechanical integrity.[12,13] A popular method for overcoming the crystallization of PEO is through cross-linking, which may also enhance thermal and chemical resistance.[7,14−16] Cross-linked polyether films can be achieved through radical polymerization of terminal (meth)acrylates or step-growth polymerization involving PEO-based macromonomers.[14,17] Although cross-linked PEO yields amorphous membrane materials, it offers few options for functionalization. Limited research has been done to create cross-linked films of other polyethers because of limited general-use synthetic techniques demonstrated for both linear and cross-linked polyether architectures. These limitations motivate the development of a new polymerization platform to explore functional polyether compositions as polymeric membranes and films. A chain-growth approach offers a versatile strategy for cross-linked materials synthesis and the opportunity for a more comprehensive exploration of polyether structure−property relationships.

A chain-growth network polymerization of epoxides can address the need for new synthetic concepts in polyether-based

Received: November 4, 2019
Revised: January 3, 2020
Published: February 3, 2020

Downloaded via UNIV OF TEXAS AT AUSTIN on May 9, 2020 at 22:10:53 (UTC).
See https://pubs.acs.org/sharingguidelines for options on how to legitimately share published articles.

ACS Publications © 2020 American Chemical Society

materials. In previous studies, we developed mono(μ-alkoxo)-bis(alkylaluminum) (MOB) initiators for epoxide polymerization with demonstrated tolerance to a range of chemical functionality, high conversion, and controlled molecular weight for some monomer systems.[18,19] In this report, we investigate the versatility of introducing a diglycidyl ether into a MOB-initiated epoxide polymerization, which represents a chain growth network polymerization resulting in a cross-linked film (Scheme 1). The composition of the epoxide monomer feed

Scheme 1. Synthesis of Cross-linked Polyether Membranes Using the $(Al(iBu_3))\cdot O(Al(iBu_2))CH_2CH_2N(CH_3)_2$ Initiator

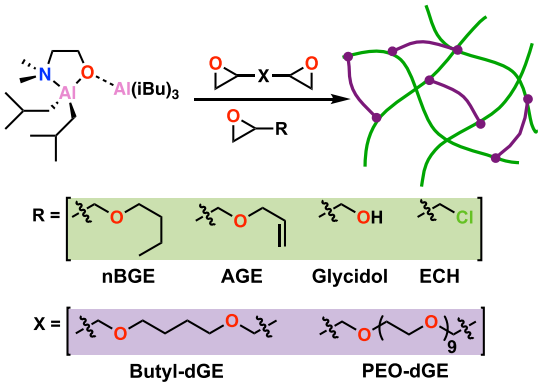

can be tuned to target diverse membrane applications. In situ kinetic ^{1}H NMR spectroscopy studies provided insight into polymerization rates and relative monomer incorporation, while membrane characterization connects polymer composition to membrane transport properties. A series of copolymerizations of *n*-butyl glycidyl ether (*n*BGE) with varying amounts of poly(ethylene oxide) diglycidyl ether (PEO-dGE) exhibited high permeability and selectivity for CO_2 in light gas separations for pure and humidified transport studies. In addition to the new synthetic concepts presented in this report, the influence of water vapor on the separation of CO_2 and N_2 using cross-linked polyether membranes has never been reported to the best of our knowledge. These amorphous, rubbery films demonstrated excellent flexibility, processability, and a direct connection between polymer composition and the resultant viscoelastic and transport properties.

EXPERIMENTAL SECTION

Materials. 2-Dimethylaminoethanol (Sigma-Aldrich, >99.5%), hexanes (Sigma-Aldrich, ACS reagent, >99.5%), triisobutylaluminum (1.0 M in hexanes, Sigma-Aldrich), epichlorohydrin (ECH) (TCI, >99%), allyl glycidyl ether (AGE) (Aldrich, ≥99%), glycidol (Aldrich, 96%), poly(ethylene glycol) diglycidyl ether (Aldrich, average M_n 500), 1,4-butanediol diglycidyl ether (Butyl-dGE) (Aldrich, ≥95%), and d_6-benzene (Cambridge Isotopes) were all used as received. *n*BGE (TCI, >98%) was dried over calcium hydride. All air and moisture sensitive reactions were prepared under a dry nitrogen atmosphere inside a glovebox. Pure gases were used as received from Air Gas Southeast Inc. Hydrogen, methane, nitrogen, oxygen, and carbon dioxide had a purity of (99.9%).

Synthesis of MOB $[(Al(iBu)_3)\cdot O(Al(iBu)_2)CH_2CH_2N(CH_3)_2]$. Details of the synthesis have been reported previously.[20] ^{1}H NMR spectroscopy (C_6D_6, 400 MHz, ppm relative to residual C_6H_6): δ −0.31 (dd, −Al[−C$\underline{H}_2$−CH−$(CH_3)_2]_3$), 0.21 (dd, −Al[−C$\underline{H}_2$−CH−$(CH_3)_2]_2$), 0.31 (m, −Al[C$\underline{H}_2$−CH−$(CH_3)_2]_2$), 1.07 (d, −Al[−CH_2−CH−(C$\underline{H}$)$_2]_3$), 1.12 (d, Al[−CH_2−CH−(C$\underline{H}_3$)$_2$]), 1.36 (d, Al−[CH_2−CH−(C$\underline{H}_3$)$_2]_2$), 1.49 (s, N−$(CH_3)_2$), 1.67 (t, N−C$\underline{H}_2$−CH_2−O), 1.96 (m, −Al[−CH_2−C$\underline{H}$−$(CH_3)_2]_2$), 2.26 (m, −Al[CH_2−C$\underline{H}$−$(CH_3)_2]_2$), 3.49 (t, N−CH_2−C$\underline{H}_2$−O), 7.16 d_6-benzene.

Kinetic ^{1}H NMR Spectroscopy Study of Copolymerization Kinetics. Kinetic ^{1}H NMR spectroscopy was performed on a 500 MHz VARIAN INOVA spectrometer at 60 °C and referenced to the residual solvent signal of C_6D_6. Two reactions were conducted using different diglycidyl ether cross-linkers, which were both copolymerized with ECH. Each polymerization was initiated in a vial containing 28.5 mg (0.067 mmol) of MOB initiator and 1 g of total monomer consisting of 10 mol % of cross-linker and 90 mol % ECH. The reactions were carried out on a 1 g scale to best resemble the actual membrane synthesis compositions. The reaction solution (0.4 mL) was transferred via a syringe into an NMR liner tube after which 0.5 mL of deuterated benzene was added to the outside of the liner for locking and shimming. The sample tube was warmed to 60 °C and the reaction was quickly placed in a NMR spectrometer. The NMR spectrometer was held at 60 °C and collected scans at periodic time intervals of 30 min. ^{1}H spectra were collected over 12 h which was sufficient for complete monomer conversion.

General Membrane Preparation. Films were all initially prepared in a 20 mL vial with the MOB initiator, epoxide monomer, and diglycidyl ether cross-linker. The reaction mixture was heated to 60 °C under a nitrogen atmosphere inside a glovebox until viscosity visibly increased (typically after 3 h). The resultant viscous solution was sandwiched between two quartz plates, which were separated by aluminum spacers to control film thickness. The plates were placed inside the antechamber of a glovebox, which was equipped with a heating stage, and left to react overnight under a nitrogen atmosphere. The solid films obtained by this process were three-dimensional networks and contained a negligible amount of material that was not bound to the network (ca. 1 wt % from Soxhlet extraction as measured in samples 5−8). Sample thickness ranged from 100 to 200 μm.

Thermal Characterization. Differential scanning calorimetry (DSC) was performed on a TA250 series analyzer (TA Instruments). A membrane (5−10 mg) was loaded in an aluminum pan and crimped with an aluminum hermetic lid. The sample was heated from −90 °C to a maximum of 250 °C with heating and cooling rates of 5 °C/min under a N_2 atmosphere. Data from the second heating curve were collected. Thermogravimetric analysis (TGA) was performed on a Mettler Toledo DSC/TGA 3+ under a N_2 atmosphere with a heating rate of 10 °C/min. Approximately 3 mg of the membrane sample was loaded in an aluminum pan and heated to a maximum of 500 °C.

Density. A Micromeritics AccuPyc II 1340 Series pycnometer was used for density measurements. The density measurements were made via helium gas displacement in a 1 cm^3 sample chamber. Samples were sealed in the sample chamber of known volume after which helium gas was admitted and then expanded into the reference chamber of a known internal volume. The differential pressures observed in the sample chamber from filling and discharging subsequently yields the sample volume using the following equation

$$V_s = V_c - \frac{V_r}{\frac{P_1}{P_2} - 1} \quad (1)$$

where V_s is the sample volume, V_c is the volume of the empty sample chamber, V_r is the volume of the reference chamber, P_1 is the pressure in the sample chamber, and P_2 is the pressure in the reference chamber.

Rheological Analysis. The viscoelastic properties of equilibrated cross-linked polyether films were determined with a TA instrument HR-2 rotational rheometer equipped with 8 mm diameter stainless steel parallel plate geometry. Oscillatory rheological measurements were conducted to measure the moduli of the films as a function of shear strain amplitude and as a function of frequency. The film sample was fixed between the upper parallel plate and stationary surface, with the gap size set according to individual film thickness (100−200 μm). All tests were performed in triplicate at 25 ± 0.1 °C. Cross-link

https://dx.doi.org/10.1021/acs.macromol.9b02318
Macromolecules 2020, 53, 1191−1198

Table 1. Characterization of MOB-Initiated Cross-linked Membranes

sample	monomer	cross-linker	[M]/[I][a]	cross-linker (wt %)	density (g/cm^3)[b]	T_g (°C)	shear modulus (MPa)[c]	cross-link density × 10^4 (mol/cm^3)[d]
1	*n*BGE	Butyl-dGE	109	14.7	1.05	−68.2	1.06	4.27
2	AGE	Butyl-dGE	122	16.4	1.12	−69.8	1.49	6.01
3	ECH	Butyl-dGE	145	19.5	1.39	−19.3	0.94	3.80
4	glycidol	Butyl-dGE	173	23.3	1.30	−4.5	1.52	6.13
5	*n*BGE	PEO-dGE	101	16.8	1.10	−71.5	0.47	1.91
6	*n*BGE	PEO-dGE	90	29.9	1.12	−67.8	0.95	3.85
7	*n*BGE	PEO-dGE	81	40.4	1.15	−62.6	1.63	6.61
8	*n*BGE	PEO-dGE	73	48.9	1.17	−58.7	2.05	8.29

[a]All the samples were prepared on a 1 g basis using 26.5 mg of MOB initiator. [b]Measured by gas pycnometry. [c]The plateau shear modulus was measured by rheometry. [d]Calculated from the shear modulus.

density (V_x) was estimated using the measured shear plateau modulus (G') and the following equations[21]

$$M_c = \frac{\rho RT}{G'} \tag{2}$$

$$V_x = \frac{\rho}{M_c} \tag{3}$$

where M_c is the average molecular weight of polymer segments between cross-links, ρ is the density of the cross-linked membrane, R is the ideal gas constant, and T is the temperature at which G' and ρ are evaluated (25 °C in our case).

Gas Permeation Measurements. The pure gas permeabilities of H_2, CH_4, N_2, O_2, and CO_2 were obtained at 35 °C using a custom-built system based on a constant volume/variable-pressure method.[22] All membranes were dried under vacuum overnight followed by overnight degassing. The upstream pressure was maintained at predetermined set values of 3.0, 6.4, 9.8, 13.0, and 16.6 atm, while the increase in the downstream pressure was recorded as a function of time. Steady-state gas permeabilities (P) were determined from the rate of pressure increase in the downstream volume using[22−24]

$$P = \frac{V_d l}{p_2 ART}\left[\left(\frac{dp_1}{dt}\right)_{ss} - \left(\frac{dp_1}{dt}\right)_{leak}\right] \tag{4}$$

where V_d is the downstream volume, l is the film thickness, p_2 is the upstream pressure, A is the area of the film accessible to gas transport, R is the gas constant, T is the temperature, $(dp_1/dt)_{ss}$ is the rate of increase in downstream pressure, and $(dp_1/dt)_{leak}$ is the leak rate of the system. The ideal selectivity was determined by taking the ratio of P for two gases using[25]

$$\alpha_{A/B} = \frac{P_A}{P_B} \tag{5}$$

The impact of humidity on N_2 and CO_2 permeabilities were determined at 35 °C using a constant pressure/variable volume apparatus equipped with a hygrometer. Gas permeability coefficients were determined at 0−75% relative humidity (RH). Helium gas was used to sweep the downstream side of the membrane and carry the permeate to a gas chromatograph (Hewlett Packard 6890 Series) equipped with a thermal conductivity detector. The partial pressure of the penetrant (i.e., N_2 or CO_2) on the downstream side was very close to zero (<0.05 atm). A sufficient residual flow rate at the upstream side was maintained to remove any helium that might permeate from the downstream side and to ensure that the feed gas was 100% N_2 or CO_2. The upstream pressure ranged from 4 to 16 atm. The permeability coefficient (P) was then calculated using the following equation[26]

$$P = \frac{x^P S(\mathrm{He}) l}{x^P_{He} A} \tag{6}$$

where x^P here is the mole fraction of either CO_2 or N_2 in the permeate stream, S(He) is the helium sweep gas flow rate, l is the membrane film thickness, x^P_{He} is the mole fraction of helium in the permeate stream, and A is the membrane area.

The film thicknesses were controlled using 100 μm spacers and membranes were between 50 and 70 μm for transport measurements. The thickness was determined within 1 μm using direct measurement with a low force digital micrometer (Litematic VL-50A series 318, Mitutoyo Corp., Japan). Standard deviations of measured thicknesses ranged from ca. 5 to 7 μm. Gas permeability measurements included errors calculated based on the standard propagation of error method.

Sorption Measurements. Gas solubility at 35 °C was determined using a dual volume, dual transducer apparatus based on the barometric, pressure decay method.[12] Polymer samples were degassed by exposure to vacuum in the sorption cell overnight before beginning sorption measurements and between each gas. For this measurement, we used the two 1000 psig Honeywell Sensotec pressure transducers (Model STJE). Long equilibration times (12 h) were performed to make the sorption measurements in the cross-linked polyether samples as accurate as possible because in this rather polar material, gas solubilities were low.

RESULTS AND DISCUSSION

Synthesis of Cross-linked Polyether Membranes. Herein, we investigated the use of the MOB initiators for the synthesis of cross-linked polyether membranes. In previous work, we explored the reactivity of MOB initiators for the polymerization of epoxide monomers into linear polyethers. The MOB initiators were shown to exhibit tolerance of chemical functionality, provide control of molecular weight, and access to high reaction rates under some conditions.[18,19] In order to further expand the generality of this synthetic technique, a range of functional monomer substrates were polymerized into cross-linked networks between quartz plates. Scheme 1 shows the general synthetic concept for the polyether membranes and the monomers that were investigated. All membrane synthesis was conducted under a dry N_2 environment inside a glovebox. The MOB initiator was first weighed in a scintillation vial followed by the addition of the epoxide monomer and a diglycidyl ether cross-linker. The reaction was then heated to 60 °C. Once the reaction mixture became apparently viscous after ca. 3 h, it was cast onto a quartz plate and sandwiched with a second quartz plate with aluminum shims to control thickness. The film was left to react overnight in a heated glovebox antechamber under nitrogen at 60 °C. Reaction conditions and characteristics of the resultant cross-linked films are summarized in Table 1. Because of the fast kinetics of polymerization for ECH and glycidol, the monomer mixtures were first cooled to 0 °C before addition of the MOB initiator. Linear polyethers that were previously

https://dx.doi.org/10.1021/acs.macromol.9b02318
Macromolecules 2020, 53, 1191−1198

synthesized using MOB initiators were colorless and exhibited optical transparency.[18−20] The newly synthesized cross-linked polyether films produced with the MOB initiators were also optically transparent in addition to being free standing and flexible, as shown in Figure 1.

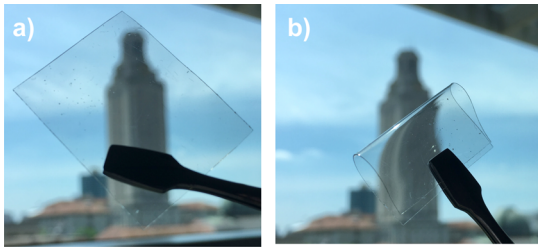

Figure 1. Images of the representative cross-linked polyether membrane demonstrating optical transparency (a) and flexibility (b).

Characterization of Reactivity Ratios with Kinetic ^{1}H NMR Spectroscopy. The cross-linked polyether membranes were created through a chain-growth network copolymerization where compositional drift may affect heterogeneity. We investigated compositional drift by in situ ^{1}H NMR spectroscopy of a model copolymerization of ECH with two different diglycidyl ether cross-linkers (^{1}H NMR spectra shown in Figure S1). ECH was chosen for this experiment because of its distinct epoxide methine signal apart from the signal of a glycidyl ether. This allowed differentiation between consumption of the epoxide monomer and the diglycidyl ether cross-linker. An NMR tube liner was used to monitor the bulk polymerization reaction conditions while isolating the deuterated solvent for locking and shimming the spectrometer (^{1}H NMR spectra shown in Figure S2). Data were collected every 30 min for 12 h and fit to extract reactivity ratios. We interpreted copolymerization kinetics shown in Figure 2 by comparing reactivity ratios derived from fits of the terminal Meyer−Lowry (ML)[27] model and the nonterminal Beckingham−Sanoja−Lynd (BSL) model.[28,29] Figure 2a,c shows the fit of BSL to the conversion as a function of unitless concentration of each monomer ($[M]/[M]_0$). Figure 2b,d shows the fit of ML to total conversion versus instantaneous mole fraction of ECH ($f_{ECH}(t)$) with respect to all epoxide functional groups in the system. The reactivity ratios for ECH (r_{ECH}) and Butyl-dGE ($r_{Butyl\text{-}dGE}$) were estimated to be r_{ECH} = 0.67 ± 0.04 and $r_{Butyl\text{-}dGE}$ = 1.39 ± 0.09 using the BSL nonterminal model, Figure 2a. By fitting the same data formatted for the ML terminal model equation we were able to extract reactivity ratios of r_{ECH} = 0.78 ± 0.33 and $r_{Butyl\text{-}dGE}$ = 1.32 ± 0.06 as shown in Figure 2b. The reactivity ratios were in agreement within the regression error between both models. This suggested that the copolymerization kinetics for ECH and Butyl-dGE could be sufficiently described using the simpler nonterminal model for compositional drift.[29] These reactivity ratios also suggested that the epoxide functional groups of Butyl-dGE were preferentially incorporated into the cross-linked network over ECH. Significantly, the copolymerization proceeded to quantitative conversion with complete and uniform incorporation of both monomers.

The BSL and ML fits to the compositional drift data for the ECH and PEO-dGE system are shown, respectively, in Figure 2c,d. The nonterminal BSL model generated reactivity ratios of r_{ECH} = 0.71 ± 0.02 and $r_{PEO\text{-}dGE}$ = 1.39 ± 0.03. The reactivity ratios that resulted from fitting to the terminal ML model were

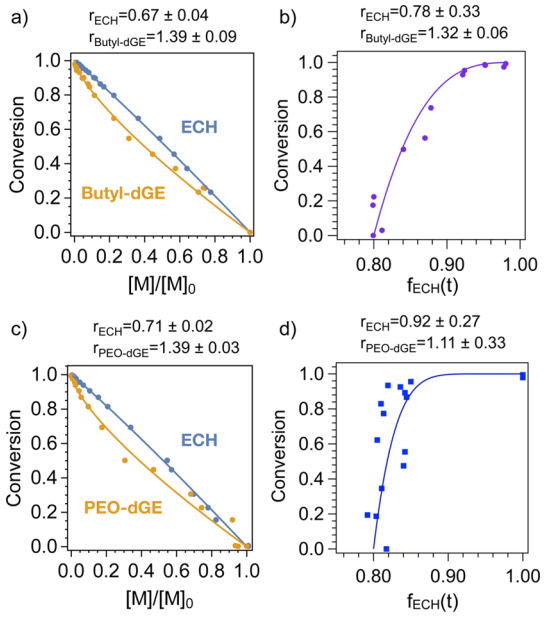

Figure 2. Reactivity ratios were extracted from fits to compositional drift data derived from ^{1}H NMR spectroscopy (600 MHz, C_6D_6) measurements of copolymerization of ECH with Butyl-dGE (a,b) and PEO-dGE (c,d) over 12 h at 60 °C. The data were fit using the nonterminal BSL model (a,c) and the terminal ML model (b,d). Reactivity ratios were consistent with nonterminal copolymerization kinetics.

r_{ECH} = 0.92 ± 0.27 and $r_{PEO\text{-}dGE}$ = 1.11 ± 0.33. Within the error of the fits, the nonterminal and terminal models again produced consistent reactivity ratios. Therefore, the simpler nonterminal model and its associated reactivity ratios provide a sufficient description of the copolymerization.[29] Compositional bias with conversion was lower in the ECH/PEO-dGE system, which achieved quantitative conversion and uniform incorporation of both monomers. Both of the copolymerizations discussed demonstrated the ability of a MOB initiator to create compositionally controlled polyether membranes with reactivity ratios close to unity and reaction kinetics consistent with the nonterminal model.

Thermal and Rheological Properties. Further evidence of compositional control of structure−property relationships in the network polyether materials was evident in the thermal and rheological properties of the resultant films. Measured and derivative values from these experiments can be found in Table 1. All of the cross-linked polyethers demonstrated high thermal stability with decomposition temperatures of 332−363 °C (Figures S3 and S4). The glass transition temperatures (T_g) of the cross-linked polyether materials were measured using DSC and can be found in Figures S5−S7. The cross-linked polyethers were rubbery and consistent with cross-linking of low T_g materials. The resultant T_g's of the cross-linked films were generally less than −50 °C. This is noteworthy because low T_g values have been shown to mitigate physical aging and promote high permeabilities in membrane materials.[15] There were also no signs of melting or crystallization in any of the films.

Rheological measurements can be utilized to provide information on viscosity, viscoelasticity, cure profiling, and cross-link density. The shear plateau storage modulus (G') is proportional to the cross-link density and serves as a connection between polymer chemistry and viscoelasticity.

https://dx.doi.org/10.1021/acs.macromol.9b02318
Macromolecules 2020, 53, 1191−1198

The average molecular weight of polymer segments between cross-links (M_c) can be found using eq 2. Dividing the membrane density (ρ) by M_c yields cross-link density (V_x) as given by eq 3. Membrane samples 5−8 offered the ability to investigate the effect of increasing the PEO-dGE cross-linker in the *n*BGE monomer feed on the resultant cross-link density (V_x).[30] Sample 5 had the lowest incorporation of PEO-dGE cross-linker at 16.8 wt % (5 mol %) with a measured G' of 0.47 MPa. Sample 8 had the highest incorporation of cross-linkers at 48.9 wt % (20 mol %) and exhibited a G' of 2.05 MPa. Table 1 contains a summary of the results and Figure 3 shows

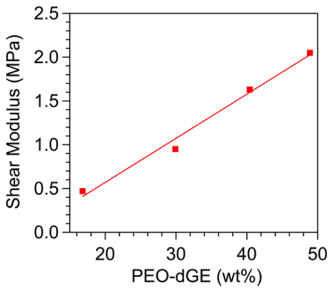

Figure 3. Direct relationship was evident between the plateau modulus (G') of the cross-linked membranes and wt % of the PEO-dGE cross-linker.

the direct linear relationship between cross-linker loading and measured G'. This linear relationship was consistent with a linear and uniform increase in cross-link density as cross-linker loading was increased in the polymerization. The uniform increase in modulus was consistent with the reactivity ratios in the model ECH/PEO-dGA and ECH/Butyl-dGA systems (vide supra Figure 2).

Gas Transport Properties. Samples 5−8 represent a series of membranes composed of *n*BGE with increasing incorporation of the PEO-dGE cross-linker and increasing cross-link density (V_x). Using the constant volume variable pressure gas permeation technique, we measured the permeability of five different test gases (H_2, N_2, O_2, CH_4, and CO_2) across samples 5−8. Pure gas permeation results were obtained at 4−16 atm feed pressure and 35 °C. Plots of test gas permeability as a function of feed pressure are provided in Figure S8−S11. The gas transport properties are summarized in Table 2. In general, the permeabilities for all gasses were similar among the materials except for CO_2, which was the most permeable gas and exhibited a substantial variation from one sample to another. PEO exhibits a high affinity for CO_2.[7] We expected that our structurally homologous membranes would also exhibit similarly high affinities for CO_2.

A trade-off typically exists between gas permeability and selectivity.[15] However, this tradeoff is not apparent in our materials. Figure 4 illustrates that permselectivity increases for

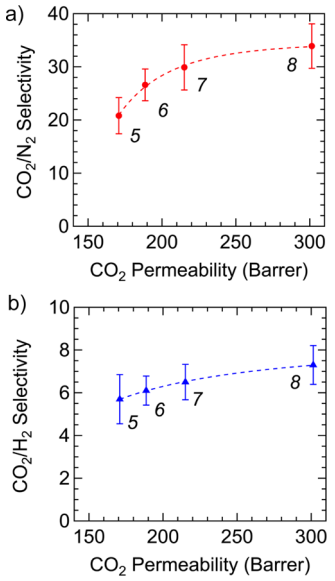

Figure 4. Relationship between CO_2 permeability and (a) CO_2/N_2 selectivity (b) CO_2/H_2 selectivity of cross-linked *n*BGE polyether membranes with varying incorporations of the PEO-dGE cross-linker. Numbers near data points denote the sample number in Table 1.

CO_2/N_2 and shows little variation for CO_2/H_2 as CO_2 permeability increases. We attributed this feature to the increase in the ether oxygen content realized from the increasing incorporation of the PEO-dGE cross-linker (Figure S12).

Transport of gas molecules through polymeric materials obeys a solution-diffusion model where gas molecules sorb into the upstream (i.e., high pressure) face of the membrane and then diffuse through and desorb from the downstream face of the membrane on the low-pressure side. Thus, permeability is given by the following[24]

$$P_A = D_A S_A \tag{7}$$

where D_A is the diffusivity coefficient and S_A is the solubility coefficient of gas molecule A in the polymer matrix. Gas permeabilities and solubilities are often measured independently and gas diffusivities can be inferred using eq 7. In order to gain a more comprehensive understanding of gas permeation in these cross-linked networks, it is helpful to decouple the diffusivity and solubility coefficients by measuring gas sorption.

Gas sorption in rubbery polymers often obeys Henry's law.[31] In Figure 5 sorption isotherms for CO_2 are well described by Henry's law over the pressure range measured. We also attempted to measure N_2 sorption, but found that the sorption levels were too low to measure accurately. CO_2 exhibited overlapping sorption isotherms as shown in Figure 5. Work

Table 2. Characteristics and Transport Properties of *n*BGE Cross-linked with PEO-dGE

		permeability (barrer)[a]					ideal selectivity ($\alpha_{x/y}$)[b]	
sample	composition	H_2	CH_4	N_2	O_2	CO_2	CO_2/N_2	CO_2/H_2
5	$P(EO_{0.17}\text{-}co\text{-}nBGE_{0.83})$	30 ± 4.3	26 ± 3.7	8.4 ± 0.7	18 ± 2.6	171 ± 24	21 ± 3.4	5.7 ± 1.1
6	$P(EO_{0.30}\text{-}co\text{-}nBGE_{0.70})$	31 ± 2.4	25 ± 1.9	7.2 ± 0.6	18 ± 1.4	189 ± 14	27 ± 3.0	6.1 ± 0.7
7	$P(EO_{0.40}\text{-}co\text{-}nBGE_{0.60})$	33 ± 3.0	25 ± 2.7	7.2 ± 0.6	19 ± 2.0	215 ± 19	30 ± 3.6	6.5 ± 0.8
8	$P(EO_{0.49}\text{-}co\text{-}nBGE_{0.51})$	41 ± 3.7	30 ± 2.7	9.0 ± 0.8	23 ± 2.0	301 ± 25	34 ± 4.1	7.3 ± 0.9

[a]Measured using the constant-volume/variable pressure method at 12 atm and 35 °C. [b]Calculated from $\alpha_{x/y} = P_x/P$.

https://dx.doi.org/10.1021/acs.macromol.9b02318
Macromolecules 2020, 53, 1191−1198

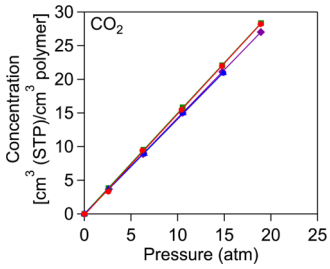

Figure 5. Sorption isotherms for CO_2 in series of cross-linked *n*BGE/PEO membranes at 35 °C. (Red dots)—sample 5, (blue triangles)—sample 6, (green squares)—sample 7, and (purple diamonds)—sample 8.

from Hirayama et al. on cross-linked PEO networks also displayed small differences in CO_2 solubility compared with those evident in permeability and diffusivity.[32] They attributed the observed large CO_2 permeabilities to large CO_2 diffusivities. These data suggest a strong positive correlation between increasing PEO content and CO_2 permeability. The absence of differences in our solubility coefficients also suggest that diffusivity is the dominant factor contributing to differences in permeability among our cross-linked networks. Thus, both composition and cross-link density were systematically varied with little effect on gas solubility.

The typical components in flue gas after desulfurization are 70% N_2, 14% CO_2, 12% H_2O, 3% O_2, and trace amounts of NO_x and SO_x.[33] Water vapor has been shown to strongly influence gas transport properties of some membranes.[34] We performed permeability measurements with CO_2 and N_2 under humidified conditions to determine the effects of water vapor in our cross-linked polyether series. Measurements at 0% RH established a comparative baseline to our previous pure gas measurements. Figure 6 presents the effect of the RH level in the feed gas on (a) CO_2 and (b) N_2 permeabilities. Interestingly, there was little measurable impact of humidity on CO_2 or N_2 permeability.

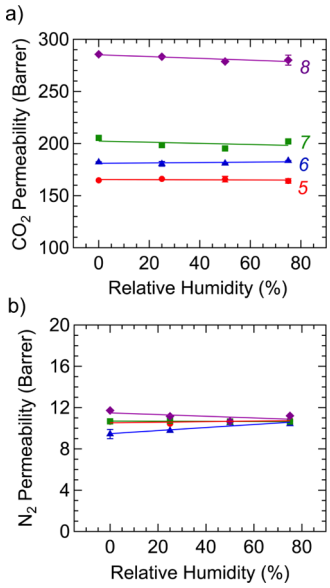

Figure 6. Effect of humidity on (a) CO_2 permeability and (b) N_2 permeability. (Red dots)—sample 5, (blue triangles)—sample 6, (green squares)—sample 7, and (purple diamonds)—sample 8.

CONCLUSIONS

We report a new synthetic approach for cross-linked polyether network materials using a MOB initiator and multifunctional epoxide monomer precursors. We utilized a range of epoxide substrates and demonstrated tolerance toward chemical functionality. The resultant cross-linked polyether films exhibited uniform and complete incorporation of comonomers into polymer films with thermal stability, optical transparency, and flexibility. The series of cross-linked *n*BGE and PEO-dGE films demonstrated relatively high CO_2 permeability and permselectivity under both dry and humidified conditions. Sorption isotherms suggested that changes in the permeability from one sample to another was driven by changes in diffusivity rather than gas solubility. CO_2 diffusivity increased as membrane cross-link density increased. The connection between materials composition and resultant static and dynamic properties demonstrates compositional control of structure−property relationships in this new synthetic materials platform.

ASSOCIATED CONTENT

Supporting Information

The Supporting Information is available free of charge at https://pubs.acs.org/doi/10.1021/acs.macromol.9b02318.

^{1}H NMR spectroscopy, TGA and DSC curves of cross-linked polyethers, pure gas permeabilities, water uptake, glass transition temperatures, and ether oxygen content for series of cross-linked *n*BGE and PEO-dGE (PDF)

AUTHOR INFORMATION

Corresponding Authors

Benny D. Freeman − *McKetta Department of Chemical Engineering, University of Texas at Austin, Austin, Texas 78712, United States;* orcid.org/0000-0003-2779-7788; Email: freeman@che.utexas.edu

Nathaniel A. Lynd − *McKetta Department of Chemical Engineering, University of Texas at Austin, Austin, Texas 78712, United States;* orcid.org/0000-0003-3010-5068; Email: lynd@che.utexas.edu

Authors

Christina G. Rodriguez − *McKetta Department of Chemical Engineering, University of Texas at Austin, Austin, Texas 78712, United States;* orcid.org/0000-0001-8681-4002

Malgorzata Chwatko − *McKetta Department of Chemical Engineering, University of Texas at Austin, Austin, Texas 78712, United States*

Jaesung Park − *McKetta Department of Chemical Engineering, University of Texas at Austin, Austin, Texas 78712, United States*

Caitlin L. Bentley − *McKetta Department of Chemical Engineering, University of Texas at Austin, Austin, Texas 78712, United States*

Complete contact information is available at: https://pubs.acs.org/10.1021/acs.macromol.9b02318

Author Contributions

The manuscript was written through contributions of all the authors. All the authors have given approval to the final version of the manuscript.

https://dx.doi.org/10.1021/acs.macromol.9b02318
Macromolecules 2020, 53, 1191−1198

Funding
Welch Foundation (F-1904). National Science Foundation (DMR-1720595).

Notes
The authors declare no competing financial interest.

■ ACKNOWLEDGMENTS

This research was funded in part by the Sandia Laboratory Directed Research and Development (LDRD) program, including student support through the Academic Alliance LDRD program (C.G.R.). The authors thank the Welch Foundation (F-1904) and a 3M Nontenured Faculty Award for partial support of this research. This research was partially supported by the National Science Foundation through the Center for Dynamics and Control of Materials: an NSF MRSEC under Cooperative Agreement no. DMR-1720595. The authors wish to thank Dr. Joan Brennecke for the use of a thermogravimetric analyzer.

■ REFERENCES

(1) Ferrier, R. C.; Pakhira, S.; Palmon, S. E.; Rodriguez, C. G.; Goldfeld, D. J.; Iyiola, O. O.; Chwatko, M.; Mendoza-Cortes, J. L.; Lynd, N. A. Demystifying the Mechanism of Regio- and Isoselective Epoxide Polymerization Using the Vandenberg Catalyst. *Macromolecules* **2018**, *51*, 1777−1786.
(2) Flory, P. J. Molecular Size Distribution in Ethylene Oxide Polymers. *J. Am. Chem. Soc.* **1940**, *62*, 1561−1565.
(3) Herzberger, J.; Leibig, D.; Langhanki, J.; Moers, C.; Opatz, T.; Frey, H. ″Clickable PEG″ via anionic copolymerization of ethylene oxide and glycidyl propargyl ether. *Polym. Chem.* **2017**, *8*, 1882−1887.
(4) Obermeier, B.; Wurm, F.; Mangold, C.; Frey, H. Multifunctional Poly(ethylene glycol)s. *Angew. Chem., Int. Ed.* **2011**, *50*, 7988−7997.
(5) Barteau, K. P.; Wolffs, M.; Lynd, N. A.; Fredrickson, G. H.; Kramer, E. J.; Hawker, C. J. Allyl Glycidyl Ether-Based Polymer Electrolytes for Room Temperature Lithium Batteries. *Macromolecules* **2013**, *46*, 8988−8994.
(6) Patterson, A. L.; Wenning, B.; Rizis, G.; Calabrese, D. R.; Finlay, J. A.; Franco, S. C.; Zuckermann, R. N.; Clare, A. S.; Kramer, E. J.; Ober, C. K.; Segalman, R. A. Role of Backbone Chemistry and Monomer Sequence in Amphiphilic Oligopeptide- and Oligopeptoid-Functionalized PDMS- and PEO-Based Block Copolymers for Marine Antifouling and Fouling Release Coatings. *Macromolecules* **2017**, *50*, 2656−2667.
(7) Lin, H.; Freeman, B. D. Gas and vapor solubility in cross-linked poly(ethylene glycol diacrylate). *Macromolecules* **2005**, *38*, 8394−8407.
(8) McGrath, A. J.; Shi, W.; Rodriguez, C. G.; Kramer, E. J.; Hawker, C. J.; Lynd, N. A. Synthetic strategy for preparing chiral double-semicrystalline polyether block copolymers. *Polym. Chem.* **2015**, *6*, 1465−1473.
(9) Patel, N.; Hunt, M.; Lingibson, S.; Bencherif, S.; Spontak, R. Tunable CO_2 transport through mixed polyether membranes. *J. Membr. Sci.* **2005**, *251*, 51−57.
(10) Wheatle, B. K.; Lynd, N. A.; Ganesan, V. Effect of Polymer Polarity on Ion Transport: A Competition between Ion Aggregation and Polymer Segmental Dynamics. *ACS Macro Lett.* **2018**, *7*, 1149−1154.
(11) Zhou, L.; Cheng, R.; Tao, H.; Ma, S.; Guo, W.; Meng, F.; Liu, H.; Liu, Z.; Zhong, Z. Endosomal pH-Activatable Poly(ethylene oxide)-graft-Doxorubicin Prodrugs: Synthesis, Drug Release, and Biodistribution in Tumor-Bearing Mice. *Biomacromolecules* **2011**, *12*, 1460−1467.
(12) Bondar, V. I.; Freeman, B. D.; Pinnau, I. Gas transport properties of poly(ether-b-amide) segmented block copolymers. *J. Polym. Sci., Part B: Polym. Phys.* **2000**, *38*, 2051−2062.
(13) Kalakkunnath, S.; Lin, H. Q.; Freeman, B. D.; Kalika, D. S. Relaxation characteristics of crosslinked poly(ethylene glycol) diacrylates and their relation to gas transport properties. *Abstr. Pap. Am. Chem. Soc.* **2005**, *230*, U3603.
(14) Kline, G. K.; Weidman, J. R.; Zhang, Q.; Guo, R. Studies of the synergistic effects of crosslink density and crosslink inhomogeneity on crosslinked PEO membranes for CO_2-selective separations. *J. Membr. Sci.* **2017**, *544*, 25−34.
(15) Kwisnek, L.; Goetz, J.; Meyers, K. P.; Heinz, S. R.; Wiggins, J. S.; Nazarenko, S. PEG Containing Thiol-Ene Network Membranes for CO_2 Separation: Effect of Cross-Linking on Thermal, Mechanical, and Gas Transport Properties. *Macromolecules* **2014**, *47*, 3243−3253.
(16) Kusuma, V. A.; Freeman, B. D.; Borns, M. A.; Kalika, D. S. Influence of chemical structure of short chain pendant groups on gas transport properties of cross-linked poly(ethylene oxide) copolymers. *J. Membr. Sci.* **2009**, *327*, 195−207.
(17) Zhao, H.-Y.; Cao, Y.-M.; Ding, X.-L.; Zhou, M.-Q.; Liu, J.-H.; Yuan, Q. Poly(ethylene oxide) induced cross-linking modification of Matrimid membranes for selective separation of CO_2. *J. Membr. Sci.* **2008**, *320*, 179−184.
(18) Rodriguez, C. G.; Ferrier, R. C.; Helenic, A.; Lynd, N. A. Ring-Opening Polymerization of Epoxides: Facile Pathway to Functional Polyethers via a Versatile Organoaluminum Initiator. *Macromolecules* **2017**, *50*, 3121−3130.
(19) Ferrier, R. C.; Imbrogno, J.; Rodriguez, C. G.; Chwatko, M.; Meyer, P. W.; Lynd, N. A. Four-fold increase in epoxide polymerization rate with change of alkyl-substitution on mono-μ-oxo-dialuminum initiators. *Polym. Chem.* **2017**, *8*, 4503−4511.
(20) Imbrogno, J.; Ferrier, R. C.; Wheatle, B. K.; Rose, M. J.; Lynd, N. A. Decoupling Catalysis and Chain-Growth Functions of Mono(μ-alkoxo)bis(alkylaluminums) in Epoxide Polymerization: Emergence of the N-Al Adduct Catalyst. *ACS Catal.* **2018**, *8*, 8796−8803.
(21) Ludovice, P. J. Structure-Property Relationships—Rubbery Polymers. In *Mechanical Properties and Testing of Polymers: An A−Z Reference*; Swallowe, G. M., Ed.; Springer Netherlands: Dordrecht, 1999; pp 238−241.
(22) Czichos, H.; Saito, T.; Smith, L. E. *Springer Handbook of Materials Measurement Methods*; Springer Berlin Heidelberg, 2007.
(23) Lin, H.; Freeman, B. D. Gas solubility, diffusivity and permeability in poly(ethylene oxide). *J. Membr. Sci.* **2004**, *239*, 105−117.
(24) Raharjo, R. D.; Lin, H.; Sanders, D. F.; Freeman, B. D.; Kalakkunnath, S.; Kalika, D. S. Relation between network structure and gas transport in crosslinked poly(propylene glycol diacrylate). *J. Membr. Sci.* **2006**, *283*, 253−265.
(25) Wiegand, J. R.; Smith, Z. P.; Liu, Q.; Patterson, C. T.; Freeman, B. D.; Guo, R. Synthesis and characterization of triptycene-based polyimides with tunable high fractional free volume for gas separation membranes. *J. Mater. Chem. A* **2014**, *2*, 13309−13320.
(26) Merkel, T.; Gupta, R. P.; Turk, B. S.; Freeman, B. D. Mixed-gas permeation of syngas components in poly(dimethylsiloxane) and poly(1-trimethylsilyl-1-propyne) at elevated temperatures. *J. Membr. Sci.* **2001**, *191*, 85−94.
(27) Liu, D.; Bielawski, C. W. Synthesis of Degradable Poly-[(Ethylene Glycol)-co-(Glycolic Acid)] via the Post-Polymerization Oxyfunctionalization of Poly(Ethylene Glycol). *Macromol. Rapid Commun.* **2016**, *37*, 1587−1592.
(28) Beckingham, B. S.; Sanoja, G. E.; Lynd, N. A. Simple and Accurate Determination of Reactivity Ratios Using a Nonterminal Model of Chain Copolymerization. *Macromolecules* **2015**, *48*, 6922−6930.
(29) Lynd, N. A.; Ferrier, R. C.; Beckingham, B. S. Recommendation for Accurate Experimental Determination of Reactivity Ratios in Chain Copolymerization. *Macromolecules* **2019**, *52*, 2277−2285.
(30) Lin, H.; Kai, T.; Freeman, B. D.; Kalakkunnath, S.; Kalika, D. S. The effect of cross-linking on gas permeability in cross-linked poly(ethylene glycol diacrylate). *Macromolecules* **2005**, *38*, 8381−8393.
(31) Blume, I.; Smit, E.; Wessling, M.; Smolders, C. A. Diffusion through Rubbery and Glassy Polymer Membranes. *Makromol. Chem., Macromol. Symp.* **1991**, *45*, 237−257.

https://dx.doi.org/10.1021/acs.macromol.9b02318
Macromolecules 2020, 53, 1191−1198

(32) Hirayama, Y.; Kase, Y.; Tanihara, N.; Sumiyama, Y.; Kusuki, Y.; Haraya, K. Permeation properties to CO_2 and N_2 of poly(ethylene oxide)-containing and crosslinked polymer films. *J. Membr. Sci.* **1999**, *160*, 87−99.
(33) Low, B. T.; Zhao, L.; Merkel, T. C.; Weber, M.; Stolten, D. A parametric study of the impact of membrane materials and process operating conditions on carbon capture from humidified flue gas. *J. Membr. Sci.* **2013**, *431*, 139−155.
(34) Dai, Z.; Løining, V.; Deng, J.; Ansaloni, L.; Deng, L. Poly(1-trimethylsilyl-1-propyne)-Based Hybrid Membranes: Effects of Various Nanofillers and Feed Gas Humidity on CO_2 Permeation. *Membranes* **2018**, *8*, 76−95.

https://dx.doi.org/10.1021/acs.macromol.9b02318
Macromolecules 2020, 53, 1191−1198